ChemPubSoc Europe

DOI: 10.1002/celc.201600402

CHEMELECTROCHEM Articles

Performance Enhancement of Reduced Graphene Oxide-Modified Carbon Electrodes for Vanadium Redox-Flow Systems

Barun Chakrabarti,*[a] Dan Nir,[b] Vladimir Yufit,[a] Farid Tariq,[a] J. Rubio-Garcia,[c] Robert Maher,[d] Anthony Kucernak,[c] P.V. Aravind,[b] and Nigel Brandon[a]

Reduced graphene oxide (rGO) suspended in an *N*,*N*′-dimethylformamide (DMF) solvent underwent electrophoretic deposition (EPD) on carbon paper (CP) electrodes. X-ray computed micro-tomography (XMT) indicates a 24% increase in the specific surface area of CP modified with rGO in comparison to the untreated sample. Furthermore, XMT confirms that the deposition also penetrates into the substrate. Raman analysis shows that the rGO deposited is more amorphous than the CP electrode. A significant reduction in charge-transfer resistance of the VO_2^+/VO^{2+} reaction is also observed (from impedance measurements) in modified samples in comparison to untreated CP electrodes.

1. Introduction

Electrophoretic deposition (EPD) is an important colloidal process for ceramic layer production and has advantages of short deposition time, simple apparatus requirements, versatility in terms of the shape of substrate, as well as little or no requirement for binder burnout because the final coating contains few or no organics.[1] Compared with other advanced shaping techniques, the EPD process is very versatile because it can be modified easily for a specific application. For example, deposition can be made on flat, cylindrical or any other shaped substrate with only minor change in electrode design and positioning. In particular, despite being a wet process, EPD offers easy control of the thickness and morphology of a deposited film through simple adjustment of the deposition time and applied potential.[2]

EPD of carbon nanotubes, which are basically graphene (GN) layers rolled up to form a cylinder, have been under investigation for more than a decade.[3,4] Over this time, EPD research on carbon nanoparticles has expanded continuously, including GN-based materials.[5] EPD has proven to be a very powerful technique to deposit GN-based materials for electrochemical energy storage applications.[4,6–8] A variety of GN-based materials have been investigated, including GN, graphene oxide (GO), thermally reduced GO, and GN with a post-reduction step to form reduced graphene oxide (rGO).

In general, nanoparticles have been used as successful electrocatalysts for electrochemical devices.[9,10] Similarly, GN has also been used as a successful electrocatalyst on carbon-based electrodes of the all-vanadium redox flow battery (VRFB).[11–13] Li and co-workers used ultrasound to deposit GO onto carbon felts and then electrochemically reduced the GO to rGO.[14] Cyclic voltammetry (CV) and electrochemical impedance spectroscopy (EIS) results displayed enhanced performance in terms of reduced charge-transfer resistance (R_{CT}) for the VO^{2+}/VO_2^+ couple from the VRFB. Likewise, Walsh et al. have recently shown an enhanced catalytic activity of glassy carbon electrodes to the VO^{2+}/VO_2^+ couple when modified with *N*-rGO-Mn_3O_4 (nitrogen doped) composite electrocatalyst.[15] Han et al. reported improved kinetics of the VO^{2+}/VO_2^+ couple by means of CV and EIS analyses on glassy carbon electrodes modified with a hybrid GO and multi-walled carbon nanotube-based electrocatalyst.[16] Other authors also found enhanced electron-transfer effects and mass transport for the vanadium redox couple when incorporating rGO as an electrocatalyst in carbon felt electrodes.[17–20]

The modification of carbon electrodes for VRFBs is not a new concept.[19] Poor charge-transfer kinetics of the VO^{2+}/VO_2^+ couple on standard carbon-based electrodes due to the rearrangement of their coordination structures[21] warrants the need for such modifications.[22] Despite that, it is not easy to find a readily available range of materials (besides carbon) that would be stable at the high potential of this

[a] Dr. B. Chakrabarti, Dr. V. Yufit, Dr. F. Tariq, Prof. N. Brandon
Department of Earth Science & Engineering, Imperial College London
South Kensington, London SW7 2AZ (UK)
E-mail: b.chakrabarti@imperial.ac.uk

[b] D. Nir, Dr. P. Aravind
Process & Energy Department, Delft University of Technology
Leeghwaterstraat 39, 2628 CB Delft (The Netherlands)

[c] Dr. J. Rubio-Garcia, Prof. A. Kucernak
Department of Chemistry, Imperial College London
South Kensington, London SW7 2AZ (UK)

[d] Dr. R. Maher
The Blackett Laboratory, Imperial College London
South Kensington, London SW7 2AZ (UK)

Supporting Information and the ORCID identification number(s) for the author(s) of this article can be found under http://dx.doi.org/10.1002/celc.201600402.

© 2016 The Authors. Published by Wiley-VCH Verlag GmbH & Co. KGaA. This is an open access article under the terms of the Creative Commons Attribution-NonCommercial License, which permits use, distribution and reproduction in any medium, provided the original work is properly cited and is not used for commercial purposes.

redox couple (1.0 V) in the presence of concentrated sulfuric acid.[15,23]

Other means reported for modifying carbon-based electrodes for VRFB applications include electrochemical oxidation, heat, chemical or plasma treatment, metals doping and so on.[19,24–30] Despite that, focus has remained on carbon felt-based electrodes and not on carbon paper (CP).[19] Several reports have shown that the effective use of respective flow fields such as serpentine or interdigitated assemblies sandwiched with CP result in lower ohmic and pressure drops for VRFBs,[31,32] although employment of carbon felts did provide the highest reported power density.[33] Therefore, it is important to understand the effect of rGO deposition on CP for the positive electrolyte of the VRFB because similar effects have already been reported for carbon felts.[14] To date, only a few studies have reported on laser enhancement,[34] CNT decoration,[35] or tungsten trioxide electro-catalyst,[36] which means that there appears to be little significant work on rGO modification of CP available in the literature. To fill this gap, this work describes a very versatile method of EPD for the preparation of CP-based rGO-modified electrodes that are analyzed in detail by CV, X-ray computed micro-tomography (XMT),[37] Brunauer–Emmett–Teller (BET) krypton adsorption, EIS and Raman spectroscopy to evaluate any performance enhancements. It is noted that this is, to our knowledge, the first report on advanced XMT-based 3D characterization of the rGO-modified CP electrodes.

2. Results and Discussion

Prior to the commencement of EPD, the CP substrate was imaged by means of scanning electron microscopy (SEM). Figure 1a shows that the CP is highly porous and has a complex three-dimensional structure of carbon fibers interwoven with one another and bound by carbon-based material (nodes) that appear as multi-layered graphite-like flakes. EPD was then conducted inside the EPD reactor (Figure S1, see the Supporting Information) at three different voltages for 30 min and resulted in various mass loading of rGO on the untreated CP (Table S1, see the Supporting Information). *N*,*N*′-Dimethylformamide (DMF) was chosen as the solvent for EPD, based on reports that indicated that deposition was most uniform when DMF was used compared with several other solvents.[5,38] Zeta potential experiments showed that rGO was positively charged in DMF and thus the CP was placed at the negative pole.

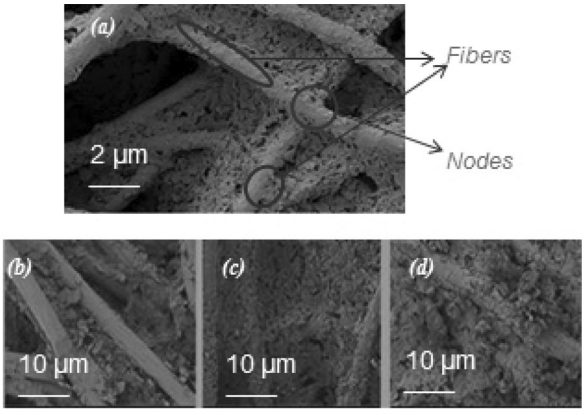


Figure 1. SEM images of CP a) untreated sample; b) with rGO deposited at 50 V; c) with rGO deposited between fibers at 300 V, and d) with rGO deposited at 700 V

As can be seen from Figure 1b, EPD at a very low value of 50 V does not result in sufficient deposition of rGO (mass loading of ca. 3% rGO). At 300 V (Figure 1c), the deposition morphology appears to be uniform (at a mass loading of ca. 10% rGO) whereas at 700 V (Figure 1d), the rGO appears to significantly block the CP pores (rGO mass loading of ca. 15% rGO).

The electrochemical performance of the rGO deposited on CP at 300 V was then evaluated towards the vanadium redox reaction (VO_2^+/ VO^{2+} redox couple) using cyclic voltammetry; the results are shown in Figure 2. The rGO modified samples

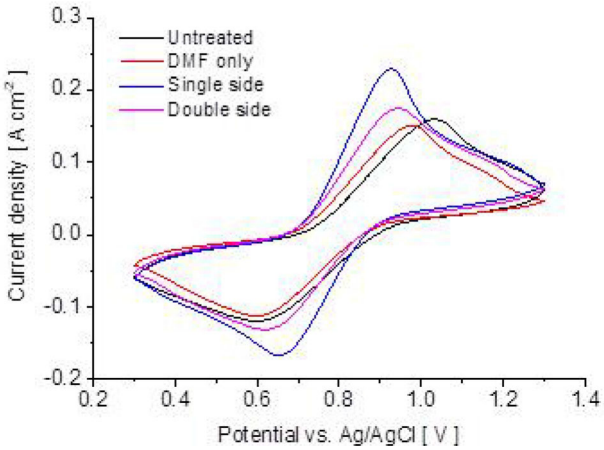


Figure 2. Electrochemical activity of untreated and rGO-modified CP (single- and double-sided deposits as well as DMF treated CP) measured by CV in 0.5 M $VOSO_4$ solution in 3 M H_2SO_4 at a scan rate of 0.025 V s^{-1}. The electrochemical reaction represents the VO_2^+/VO^{2+} redox couple.[39]

clearly show better performance in terms of higher peak current densities as well as a reduction–oxidation peak separation (Figure S2 in the Supporting Information). The DMF treatment also appeared to change the active electrochemical surface in a positive way (slightly smaller peak separation but peak current densities did not vary) but this effect has not been quantified in this work and will be reported in the future. The deposits of rGO on both sides of CP also gave better performance than untreated and DMF treated samples but could not reach that of the single-sided rGO deposited sample. This result suggests that the presence of excess rGO most likely blocks the pores of the CP and does not allow sufficient permeation of the vanadium electrolyte for the electron-transfer reaction to occur (thus reducing active electrochemical surface). However, the performance of the double-sided deposits of rGO was still better than that for the untreated CP, thereby confirming an increased active electrochemical surface of the rGO-modified electrodes with respect to the VO_2^+/VO^{2+} redox couple.

The peak currents for the VO_2^+/VO^{2+} redox couple increase significantly in the presence of rGO not only because of en-

© 2016 The Authors. Published by Wiley-VCH Verlag GmbH & Co. KGaA, Weinheim

hanced surface area but also probably because of better electronic conductivity (rGO is known to conduct electrons better than carbon).[40] This was confirmed by EIS experiments that showed lower series resistances for rGO modified CP samples than untreated ones (discussed in the following paragraphs and displayed in Table 1). Moreover, rGO reduced the hydrophobicity of the electrode as evidenced by wetting experiments using vanadium based electrolytes (Figure S3, Supporting Information); the latter permeated into the modified electrode within seconds compared with the untreated CP that took about 30 min to absorb the electrolyte. The effect of some oxygenated functional groups (provided by rGO) appears to play a significant role, as confirmed by Di Blasi et al.[41]

Table 1. Conditions for EPD on CP samples and the resulting change in electrochemical performance.

CP sample	Time [min]	rGO conc. [mg L^{-1}]	Deposition sides	R_S[a] [Ω cm^2]	R_{CT}[b] [Ω cm^2]	ΔR_{CT} [%]
untreated	–	–	–	0.5	6.5	0
single-sided rGO	30	100	1	0.3	2.6	−60.5
double-sided rGO	30[c]	100	2	0.2	4.1	−37.4
only DMF treated	30	0	1	0.4	5.2	−19.4

[a] R_S = area specific series resistance. [b] R_{CT} = charge transfer resistance calculated from electrochemical impedance spectroscopy. [c] ×2 refers to EPD on both sides of CP performed for 2×30 min.

EIS spectra of three different CP samples, namely: 1) untreated, 2) subjected to EPD in pure DMF, and 3) subjected to EPD in a solution of rGO + DMF, in a solution of 0.5 M $VOSO_4$ in 3 M H_2SO_4, are presented in Figure 3a. EIS was performed under OCV conditions at 0.8 V vs. Ag/AgCl. The diameter of the semi-depressed circle is smallest for the CP treated with rGO. The electrochemical response of the three different samples can be fitted with a modified Randles circuit in which the capacitor is replaced by a constant-phase element to account for the porous nature of the CP (inset in Figure 3a).

According to this simple circuit, R_S is the bulk resistance mainly associated with the ionic electrolyte and electronic carbon paper conductivities, R_{CT} is the diameter of the semi-depressed circle and corresponds to the charge-transfer process at the CP/electrolyte interface (corresponding to the VO^{2+}/VO_2^+ reaction), W_S is the generalized Warburg impedance for finite diffusion of the reacting species, and CPE is the constant-phase element characterizing a double-layer capacitance effect of non-ideal porous media such as the CP. Thus, Figure 3b depicts the variation in charge-transfer resistance for the VO_2^+/VO^{2+} reaction as a result of different treatments on the CP electrode.

Clearly, all treatments have a positive effect on reducing the resistance associated with charge transfer. The effect of DMF treatment alone (labeled as "no rGO" in Figure 3b) appears to reduce the hydrophobicity of the CP, which is confirmed by drop test experiments using 3 M sulfuric acid. The effect of rGO treatment is much more significant because it reduces the charge-transfer resistance of the CP by more than 60% (Table 1). This reduction is associated with increased active electrochemical surface area and wettability (there may also be some contribution of lower resistivity, R_S), due to deposited particles of rGO (supporting the results from CV). Although the double-sided deposition did reduce the charge-transfer resistance, its value was still greater than that of the one-sided deposition.

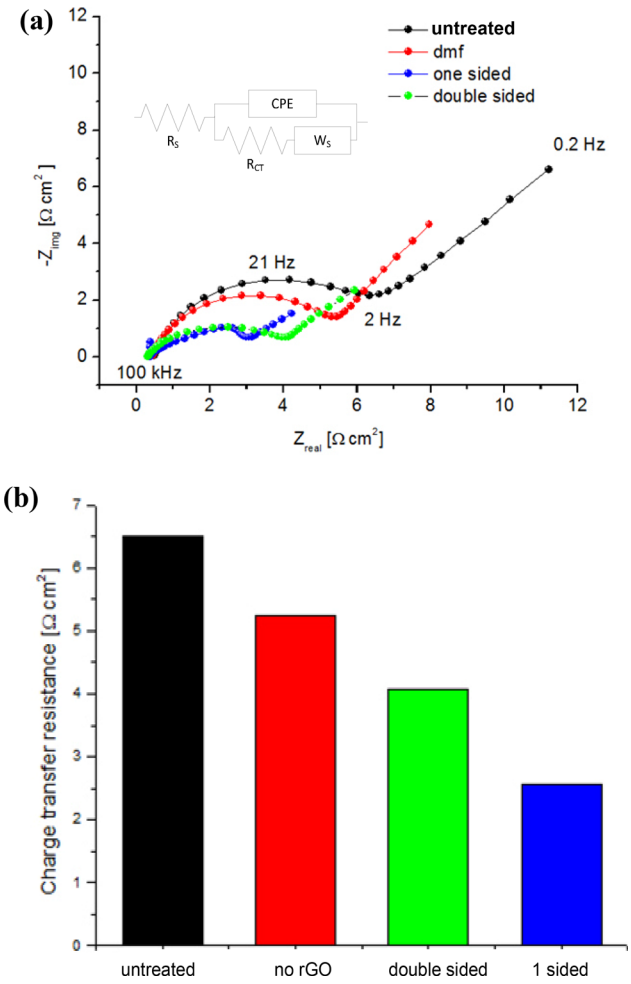


Figure 3. a) Area specific electrochemical impedance spectra of treated and untreated carbon papers; b) Area specific charge transfer resistance of treated and untreated carbon papers determined from EIS analyses. EIS was obtained in a solution of 0.5 M $VOSO_4$/ 3 M H_2SO_4 solution at 0.8 V (vs. Ag/AgCl) from 10^5 to 10^{-2} Hz by applying an AC voltage of 5 mV amplitude. Note that "no rGO" means that the untreated CP was subjected to EPD without any rGO present in the DMF solvent.

A double-sided rGO deposit increased the total surface area (as measured by BET; Table 2) but at the same time decreased the amount of accessible electrochemically active surface as a result of thicker deposition. As a consequence, the single-sided deposit, resulting in thinner deposition of rGO, gave the best performance in terms of lowering charge-transfer resistance.

Reconstructed 3D XMT images of the CP with rGO deposits (at 300 V) are displayed in Figure 4, in which a single-sided deposit is compared with a double-sided deposit as well as with an untreated CP sample. The tomograms of the untreated CP

© 2016 The Authors. Published by Wiley-VCH Verlag GmbH & Co. KGaA, Weinheim

Table 2. Changes in porosity and specific surface area of CP after deposition of rGO at 300 V (for both one- and double-sided depositions).

CP sample	Graphite flakes on nodes and carbon from deposition [vol.%][b]	Total specific surface area [$\mu m^2 \mu m^{-3}$][c]	BET specific surface area [$\mu m^2 \mu m^{-3}$][d]
untreated CP[a]	0.95	0.81	2.8
deposition on one side	1.79	1.00	5.1
deposition on two sides	2.05	1.11	11.1

[a] The dataset for untreated CP was acquired at 1.8 μm voxel size. The other datasets were acquired at 1.4 μm voxel size. [b] All data have a volumetric error of ±0.1%. [c] Determined from XMT. [d] Determined from BET analysis using Kr as probe gas.

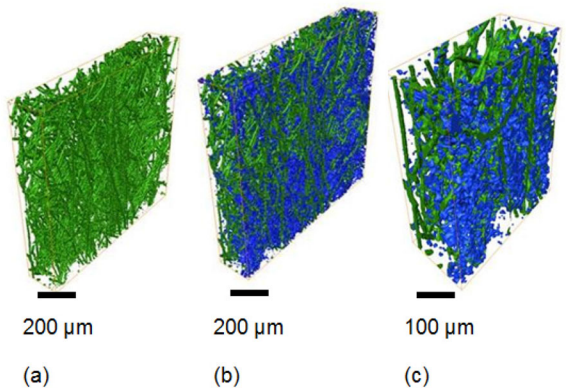


Figure 4. The reconstructed 3D XMT images of CP with and without rGO deposited by means of EPD. a) Untreated CP (green); b) rGO deposited on one side (rGO in blue); and c) rGO deposited on both sides.

and a single-sided rGO deposit are shown in Figure S4 (see the Supporting Information). The images in Figure 4 show that the EPD process produced noticeably different samples (a video highlighting the rGO deposits is given in the Supporting Information, Video V1). The changes in porosity and volume-specific surface area are shown in Table 2 based on 3D XMT data acquired with isotropic voxel resolutions of 1.4 μm. Pore-size distributions for both the untreated CP as well as a single-sided deposited sample can be found in Figure S5 (see the Supporting Information) at the given resolution. It is clear that both specific and electrochemical surface areas increased after deposition of rGO on the CP. The same trend is confirmed by BET data, although these values are about an order of magnitude larger than XMT data.

As seen from Table 2, the EPD process leads to increased amount of carbon flakes deposited on the carbon fibers of the CP. Clearly, double-sided deposition of rGO is characterized by a greater amount of graphite flakes, with higher specific surface area estimated based on an analysis of 3D dataset at the given resolution as well as BET. Nevertheless, charge-transfer resistances of single- and double-sided deposited CPs follow an opposite trend, whereby the value is larger for a double-sided electrode (indicating worse electrochemical performance for the VO_2^+/VO^{2+} couple in comparison to a single-sided deposited sample). It is likely that under the given conditions, the double-sided deposition, while increasing the total surface area of deposited rGO, reduces the active electrochemical surface for the VO^{2+}/VO_2^+ reaction (by blocking small pores <1 μm in size) in comparison to the single-sided deposited CP. The effect of enhanced electrochemical surface due to rGO deposition is also confirmed from insignificant resistivity (R_S) changes, as displayed in Table 1.

When a deposition on both sides was performed, the second deposition side appeared to be optically darker. Hence, Raman was used to examine both the quality of the deposited film, and whether the order of deposition had an effect. Raman analysis was performed on four surfaces of three samples: Untreated CP; CP with rGO deposited on one side; CP with rGO deposited on both sides (the 1st deposition side); and CP with rGO deposited on both sides (the 2nd deposition side). Based on XMT data, the rGO fully penetrates the CP with a certain gradient across the CP thickness. There seems to be little difference in the Raman peaks of the carbon formed on the 1st and 2nd deposition sides of the sample that was exposed to two EPD runs with rGO (Figure 5). These spectra

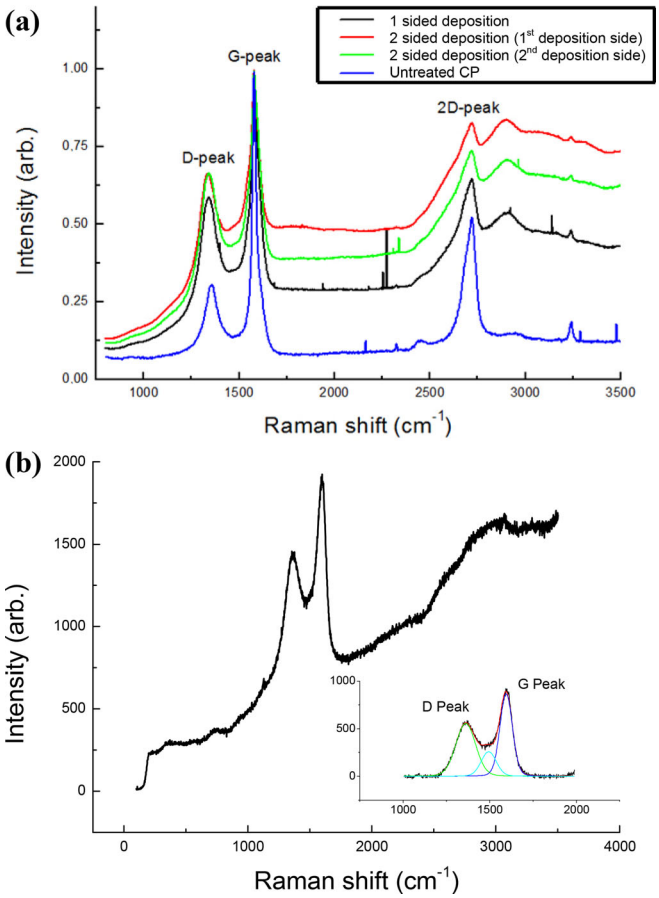


Figure 5. a) Average Raman responses generated from 40+ spectra collected from each sample, which are subcategorized as; the 300 V samples with one-sided deposition, two-sided depositions (1st and 2nd deposition sides) and untreated CP. All spectra were collected by using a 514 nm laser; (b) Average of four spectra collected of rGO nanoparticles dried on a glass slab from a DMF solution. Raman data were fitted as given in the inset below the main figure.

© 2016 The Authors. Published by Wiley-VCH Verlag GmbH & Co. KGaA, Weinheim

show the characteristic Raman signature of carbon, which includes the D peak at 1350 cm^{-1}, G peak at 1580 cm^{-1}, and 2D peak at 2700 cm^{-1}, as labeled. The D peak is the result of defects within the crystal structure of the carbon such as vacancies or the presence of foreign atoms that substituted carbon, dangling bonds and edge defects.[42] The G peak is closely related to the quality of the crystal structure as it is a fundamental mode. The 2D peak is a second-order resonance mode. As a result of the intimate dependence on the properties of the crystal structure, the relative intensity or the intensity ratio of the D and G bands is a measure of disorder, as expressed by the sp^3/sp^2 hybridized carbon bonds ratio.[43] High D/G ratios are indicative of highly defective crystal structures, with the ratio decreasing as the carbon becomes more graphitic. The width of the Raman peaks is also an indicator, albeit one that is less sensitive than the D/G intensity ratio, to the quality of the crystal structure. Any inhomogeneity in the crystal structure will lead to a broadening of the characteristic Raman features. However, because the width of the Raman modes is typically relatively small, the width is not always a reliable measure of the disorder within the crystal structure of a material under investigation but rather a supporting indicator.

In this case, the D peak is significantly smaller than the G peak for the spectra shown in Figure 5a, whereas the peaks appear to be clearly indicating that the samples are all relatively graphitic. However, there appears to be significant variation in the spectra obtained from the different samples, which allow a direct comparison. For example, the samples that were subjected to EPD using rGO appear to have a much higher D/G peak ratio than the untreated sample. The 2D peak becomes progressively broader as the sample is exposed to the deposition procedure (this is confirmed from the Raman peaks of the rGO powder on its own placed on a glass slide, which suggests an amorphous structure; Figure 5b).

The characteristics of the Raman modes, as determined by fitting the spectra shown in Figure 5, are summarized in Table 3. The intensity ratios for all the samples measured by means of Raman spectroscopy are included. The untreated CP has a much lower ratio relative to the treated samples, indicating that it is significantly more graphitic in nature. The ratio increases with the amount of rGO deposited on the CP. This suggests that the carbon deposited is more amorphous than the underlying surface. The Raman modes tend to become broader as more carbon is deposited, supporting this observation.

3. Conclusions

EPD was used to modify carbon paper electrodes with rGO nanoparticles. DMF was employed as the solvent and EPD was performed at 300 V at an inter-electrode distance of 15 mm. The enhanced electrodes showed clear deposits of amorphous structures that improved the electrochemical performance of the V^{IV}/V^{V} redox couple (as evidenced by a significant reduction in the charge-transfer resistance of rGO modified CP by ca. 60%). Improved surface area of CP due to rGO deposition was confirmed by means of XMT and BET, which reveal a higher active electrochemical surface area in the presence of rGO. XMT images also show that the rGO nanoparticles penetrate the carbon paper sufficiently to improve its specific surface area. The wettability of vanadium sulfate and sulfuric acid, which is the electrolyte of the all-vanadium redox flow battery, is far better for the rGO-modified electrode than that of the untreated carbon paper. This indicates that an optimized rGO-modified electrode could improve the efficiency and power density of the all-vanadium redox flow battery. This will be addressed in future work.

Experimental Section

Materials

CP electrodes (GDL 10 AA Series Gas Diffusion Layer) were sourced from SGL Carbon Ltd. Reduced graphene oxide (rGO) was purchased from ACS Material (USA) and used as received. *N*,*N*′-dimethylformamide (DMF) was purchased from VWR International (AnalaR NORMAPUR grade). Sulfuric acid (95% pure) and vanadium sulfate (99.9% metals basis) were also sourced from VWR International for electrochemical experiments. The working electrodes for cyclic voltammetry (CV) experiments were the samples prepared by EPD, whereas the counter electrode was a platinum foil (Goodfellow UK). An Ag/AgCl leak-free reference electrode (Warner Instruments) was used for cyclic voltammetry and impedance experiments.

Electrophoretic Deposition Reactor and Process

Because of the use of corrosive organic chemicals, the reactor was made of PTFE. Two ends were made of glass so that it was possible to observe the EPD process during experimental runs. An image of the EPD reactor is shown in Figure S1 (see the Supporting Information). The reactor was designed in a 3D CAD computer program (Solid Works) and built with a CNC machine (Techsoft). The EPD was performed horizontally, as opposed to the traditional vertical

Table 3. Numerical results from fitting Raman spectra shown in Figure 5.

Sample	D peak			G peak			
	I[a]	*P*[b]	*W*[c]	*I*	*P*	*W*	Ratio
untreated carbon paper	0.194	1354.8	55.2	0.832	1580.7	27.4	0.23
one side	0.299	1339.6	85.1	0.627	1583.2	40.6	0.48
two sides (1st deposition side)	0.269	1334.1	83.6	0.481	1582.4	41.8	0.56
two sides (2nd deposition side)	0.313	1339.6	89.0	0.558	1584.5	44.6	0.56

[a] *I* = intensity. [b] *P* = peak. [c] *W* = width.

© 2016 The Authors. Published by Wiley-VCH Verlag GmbH & Co. KGaA, Weinheim

method, because this was found to result in more uniform deposits.[44]

During EPD, potentials between 0 and 300 V were applied by means of a high-voltage power supply (EA Elektro-Automatik, EA-PS 9750-04 2U). rGO (0.1 g L^{-1}) was ultrasonically dispersed in DMF for about 2 h as reported previously.[45] CP was used as the working electrode (upper part of the reactor) and a graphite plate functioned as the counter (lower part). 15 mm inter-electrode distance was used, as reported elsewhere.[44–46] This distance enabled placement of a light source to detect any effervescence that may have impeded the EPD process (also rGO movement in the DMF due to the applied electric field could be observed). Initial experiments to determine the charge of rGO in DMF solvent was performed by measuring zeta potentials. Zeta potentials were measured with a Brookhaven PALS Zeta Potential Analyzer (version 3.48). rGO + DMF samples were diluted to 1/50th their original concentrations. All measurements were performed in triplicate at RT and pressure and the mean was estimated by the PALS Zeta potential analyzer software.

The charge of rGO in DMF was found to be positive. Subsequent EPD was performed at 300 V by placing the CP sample at the top of the reactor (this ensured a good mass loading and uniform coverage of the CP surface with rGO, as explained in the Results section). Four samples were prepared for characterization and were labeled as: 1) untreated sample; 2) no rGO (meaning CP that was subjected to EPD without any rGO particles suspended in the DMF solvent); 3) one-sided rGO deposit; 4 a) double-sided rGO deposit (1st deposition side); and 4 b) double-sided rGO deposit (2nd deposition side).

Untreated CP electrodes were initially cleansed by rinsing with acetone thoroughly prior to all EPD runs. The weights of the untreated and treated samples were measured with a mass balance (Sartorious) with an accuracy of $\pm$0.1 mg. The mass loadings of rGO on the CP were calculated from the difference in weights of treated and untreated samples and taking the percentage of the value with respect to the original weight of the untreated CP.

Cyclic Voltammetry and Impedance Measurements

For evaluating the electrochemical characteristics of the rGO deposited CP samples, a three-electrode glass cell was employed and nitrogen gas (BOC, 99.99% pure) was used to deaerate the electrolytes.[28] A leak-free Ag/AgCl electrode was employed as the reference (Warner Instruments), and a platinum wire was used as the counter electrode (Goodfellow). The CP samples (or rGO modified CP samples) were used as the working electrode, connected to a platinum plate as current collector. A 0.5 M $VOSO_4$ solution in 3 M H_2SO_4 was employed as the aqueous electrolyte;[47] all the electrodes were soaked in this for 9 h prior to investigation. To determine the electrochemical activity,[28,48] several cyclic voltammetry (CV) experiments were performed between -0.4 and 1.2 V at several scan rates ranging from 2 to 50 mV s^{-1} in a similar manner to that reported previously.[28]

Electrochemical impedance spectroscopy (EIS) at open-circuit voltage from 10^5 to 10^{-2} Hz (by applying an AC voltage of 5 mV amplitude) was used to determine the electrochemical performance of treated and untreated CP electrodes.[28] The solutions were prepared with deionized water and potentials have been reported with respect to the Ag/AgCl leak-free reference. All the electrochemical measurements were performed at ambient temperature with an Autolab potentiostat (model PGSTAT 12/30/302 supplied by Metrohm) by means of Nova software that also functioned as the data logger. The EIS fitting was carried out with Z-View software (Scribner) using a Levenberg–Marquardt minimization algorithm.[39]

Instrumentation and Characterization

Scanning electron microscopy (SEM) on the untreated and rGO-modified carbon paper samples was conducted with an Auriga-45-24 (FIBSEM) microscope with an accelerating voltage of 5 kV (pixel size = 29.46 nm). BET analysis was performed to gain information on the surface area using a Micromeritics BET Tristar II instrument and krypton (Kr) as the gas probe.[49] Nitrogen was not employed because the surface areas of the CP samples were not high enough to allow accurate measurements.

Raman spectra of untreated and modified CP samples were recorded with a Renishaw 2000 CCD (charge-coupled device) spectrometer equipped with an Olympus BH-2 confocal microscope. Spectra were collected with either an Argon ion 514 nm, a HeNe at 633 nm, or an infrared diode at 780 nm laser as excitation. The laser excitation was focused onto the sample surface using either $\times$20 or $\times$50 high numerical aperture microscope objectives, resulting in a spot size of either ca. 1.5 or 4 μm diameter. All spectra shown in this work were collected with the 514 nm laser excitation source with power in the range of 0.5–5.0 mW at the focal point. Incident power levels were limited to a power density of less than 0.1 mW μm^{-2} to ensure that no laser damage of the surface occurred during the measurements. Over 40 spectra were collected from random locations on each sample to ensure they were characterized in a statistically meaningful way. Spectra were normalized, averaged, background-corrected and fitted using a combination of Peak Fit 4.2, Renishaw wire 2.0 and Origin 8.6.

X-ray tomography (3D micro-CT or XMT) involves using an X-ray beam to produce a series of transmission projection images of an object as it is rotated though multiple angles. The resulting contrast in each acquired image is a function of the attenuation coefficients or interference effects of the phases through which the X-ray is transmitted.[37] Both untreated and modified carbon papers were mounted upright in a ceramic holder with a polymer support. XMT imaging was subsequently conducted with a GE Nanotom S Laboratory Source. A field of view of ca. 2304 $\times$ 2304 $\times$ 400 μm was reconstructed with ca. 3600 transmission images taken over a 360° rotation using 80 kV incident X-ray beam voltages. The transmission images were reconstructed by using a standard parallel beam filtered back-projection algorithm (GE Reconstruction) producing a final dataset with isotropic voxel size of ca. 1.4 μm following alignments and reconstruction.

Image analysis techniques had to be applied to segment and quantify the 3D imaged data. The acquired images were segmented based on threshold values determined manually. This was carried out both at an upper and lower boundary threshold, facilitating the selection of genuine data over the presence of noise. Once determined, the 3D structure was visually displayed and both surface areas and volumes calculated. These steps were carried out using commercially available software (Avizo, FEI, France). More comprehensive information regarding the segmentation procedures for X-ray data based on carbon electrodes are beyond the scope of the present work and can be found in a study by Tariq et al.[37]

© 2016 The Authors. Published by Wiley-VCH Verlag GmbH & Co. KGaA, Weinheim

Data Statement

Data underlying this paper can be accessed at: (10.1002/celc.201600402) or (http://hdl.handle.net/10044/1/40500).

Acknowledgements

The authors are grateful for the funding provided by the EPSRC project Lower Cost and Longer Life Flow Batteries for Grid Scale Energy Storage (EP/L014289/1). D.N.. is much obliged to Climate-Kic for providing him funds to conduct this project at Imperial College London. Dr. Mahmoud Ardakani and Dr. Ekatarina Weir are gratefully thanked for their expertise, discussion and training in SEM analyses. D.N. would also like to thank Dr. Billy Wu and Miss Harini Hewa Dewage for help with experiments in the lab. Authors would also like to acknowledge IQM Elements for providing assistance with image processing and quantification.

Keywords: cyclic voltammetry · electrophoresis · fuel cells · graphene · surface analysis

[1] L. Besra, M. Liu, *Prog. Mater. Sci.* **2007**, *52*, 1 – 61.
[2] M. S. Ata, Y. Liu, I. Zhitomirsky, *RSC Adv.* **2014**, *4*, 22716 – 22732.
[3] C. Du, D. Heldbrant, N. Pan, *Mater. Lett.* **2002**, *57*, 434 – 438.
[4] M. H. Chakrabarti, C. T. J. Low, N. P. Brandon, V. Yufit, M. A. Hashim, M. F. Irfan, J. Akhtar, E. Ruiz-Trejo, M. A. Hussain, *Electrochim. Acta* **2013**, *107*, 425 – 440.
[5] A. Chavez-Valdez, M. S. P. Shaffer, A. R. Boccaccini, *J. Phys. Chem. B* **2013**, *117*, 1502 – 1515.
[6] S. Liu, J. Ou, J. Wang, X. Liu, S. Yang, *J. Appl. Electrochem.* **2011**, *41*, 881 – 884.
[7] Y. Huang, H. Liu, Y. C. Lu, Y. Hou, Q. Li, *J. Power Sources* **2015**, *284*, 236 – 244.
[8] V. H. Nguyen, J. J. Shim, *J. Power Sources* **2015**, *273*, 110 – 117.
[9] Y. Holade, A. B. Engel, S. Tingry, A. Cherifi, D. Cornu, K. Servat, T. W. Napporn, K. B. Kokoh, *ChemElectroChem* **2014**, *1*, 1976 – 1987.
[10] T. Saida, O. Sekizawa, N. Ishiguro, M. Hoshino, K. Uesugi, T. Uruga, S.-i. Ohkoshi, T. Yokoyama, M. Tada, *Angew. Chem. Int. Ed.* **2012**, *51*, 10311 – 10314; *Angew. Chem.* **2012**, *124*, 10457 – 10460.
[11] M. H. Chakrabarti, S. A. Hajimolana, F. S. Mjalli, M. Saleem, I. Mustafa, *Arabian J. Sci. Eng.* **2013**, *38*, 723 – 739.
[12] M. Ulaganathan, V. Aravindan, Q. Yan, S. Madhavi, M. Skyllas-Kazacos, T. M. Lim, *Adv. Mater. Interfaces* **2016**, *3*, 1500309 – 1500331.
[13] M. Park, J. Ryu, J. Cho, *Chem. Asian J.* **2015**, *10*, 2096 – 2110.
[14] W. Li, J. Liu, C. Yan, *Carbon* **2013**, *55*, 313 – 320.
[15] A. Ejigu, M. Edwards, D. A. Walsh, *ACS Catal.* **2015**, *5*, 7122 – 7130.
[16] P. Han, Y. Yue, Z. Liu, W. Xu, L. Zhang, H. Xu, S. Dong, G. Cui, *Energy Environ. Sci.* **2011**, *4*, 4710 – 4717.
[17] M. Park, I.-Y. Jeon, J. Ryu, J.-B. Baek, J. Cho, *Adv. Energy Mater.* **2015**, *5*, 1401550 – 1401556.
[18] C. Flox, J. Rubio-Garcia, R. Nafria, R. Zamani, M. Skoumal, T. Andreu, J. Arbiol, A. Cabot, J. R. Morante, *Carbon* **2012**, *50*, 2372 – 2374.
[19] M. H. Chakrabarti, N. P. Brandon, S. A. Hajimolana, F. Tariq, V. Yufit, M. A. Hashim, M. A. Hussain, C. T. J. Low, P. V. Aravind, *J. Power Sources* **2014**, *253*, 150 – 166.
[20] Z. González, C. Botas, P. A 'lvarez, S. Rolda 'n, C. Blanco, R. Santamaria, M. Granda, R. Menéndez, *Carbon* **2012**, *50*, 828 – 834.
[21] J. Jin, X. Fu, Q. Liu, Y. Liu, Z. Wei, K. Niu, J. Zhang, *ACS Nano* **2013**, *7*, 4764 – 4773.
[22] M. Park, Y.-j. Jung, J. Kim, H.-i. Lee, J. Cho, *Nano Lett.* **2013**, *13*, 4833 – 4839.
[23] M. Rychcik, M. Skyllas-Kazacos, *J. Power Sources* **1987**, *19*, 45 – 54.
[24] W. H. Wang, X. D. Wang, *Electrochim. Acta* **2007**, *52*, 6755 – 6762.
[25] L. Yue, W. Li, F. Sun, L. Zhao, L. Xing, *Carbon* **2010**, *48*, 3079 – 3090.
[26] W. Li, J. Liu, C. Yan, *Carbon* **2011**, *49*, 3463 – 3470.
[27] W. Li, J. Liu, C. Yan, *Electrochim. Acta* **2011**, *56*, 5290 – 5294.
[28] C. Flox, M. Skoumal, J. Rubio-Garcia, T. Andreu, J. R. Morante, *Carbon* **2013**, *60*, 280 – 288.
[29] C. Flox, C. Fàbrega, T. Andreu, A. Morata, M. Skoumal, J. Rubio-Garcia, J. R. Morante, *RSC Adv.* **2013**, *3*, 12056 – 12059.
[30] C. Flox, J. Rubio-Garcia, M. Skoumal, J. Vázquez-Galván, E. Ventosa, J. R. Morante, *ChemPlusChem* **2015**, *80*, 354 – 358.
[31] Q. H. Liu, G. M. Grim, A. B. Papandrew, A. Turhan, T. A. Zawodzinski, M. M. Mench, *J. Electrochem. Soc.* **2012**, *159*, A1246 – A1252.
[32] R. M. Darling, M. L. Perry, *J. Electrochem. Soc.* **2014**, *161*, A1381 – A1387.
[33] Q. Zheng, F. Xing, X. Li, T. Liu, Q. Lai, G. Ning, H. Zhang, *J. Power Sources* **2014**, *266*, 145 – 149.
[34] I. Mayrhuber, C. R. Dennison, V. Kalra, E. C. Kumbur, *J. Power Sources* **2014**, *260*, 251 – 258.
[35] M. P. Manahan, Q. H. Liu, M. L. Gross, M. M. Mench, *J. Power Sources* **2013**, *222*, 498 – 502.
[36] C. Yao, H. Zhang, T. Liu, X. Li, Z. Liu, *J. Power Sources* **2012**, *218*, 455 – 461.
[37] F. Tariq, V. Yufit, M. Kishimoto, P. R. Shearing, S. Menkin, D. Golodnitsky, J. Gelb, E. Peled, N. P. Brandon, *J. Power Sources* **2014**, *248*, 1014 – 1020.
[38] Y. Hernandez, V. Nicolosi, M. Lotya, F. M. Blighe, Z. Sun, S. De, I. T. McGovern, B. Holland, M. Byrne, Y. K. Gun'Ko, J. J. Boland, P. Niraj, G. Duesberg, S. Krishnamurthy, R. Goodhue, J. Hutchison, V. Scardaci, A. C. Ferrari, J. N. Coleman, *Nat. Nanotechnol.* **2008**, *3*, 563 – 568.
[39] C. Flox, M. Skoumal, J. Rubio-Garcia, T. Andreu, J. R. Morante, *Appl. Energy* **2013**, *109*, 344 – 351.
[40] V. B. Mohan, R. Brown, K. Jayaraman, D. Bhattacharyya, *Mater. Sci. Eng. B* **2015**, *193*, 49 – 60.
[41] A. Di Blasi, O. Di Blasi, N. Briguglio, A. S. Aricò, D. Sebastián del Río, M. J. Lázaro Elorri, G. Monforte, V. Antonucci, *J. Power Sources* **2013**, *227*, 15 – 23.
[42] R. C. Maher, V. Duboviks, G. J. Offer, M. Kishimoto, N. P. Brandon, L. F. Cohen, *Fuel Cells* **2013**, *13*, 455 – 469.
[43] A. C. Ferrari, J. Robertson, *Phys. Rev. B* **2000**, *61*, 14095 – 14107.
[44] J. H. Dickerson, A. R. Boccaccini, *Electrophoretic Deposition of Nanomaterials*, Springer, New York, **2012**, pp. 181 – 215.
[45] J. Liu, B. Zeng, Z. Wu, H. Sun, *ACS Appl. Mater. Interfaces* **2012**, *4*, 1219 – 1224.
[46] L. Tang, H. Feng, J. Cheng, J. Li, *Chem. Commun.* **2010**, *46*, 5882 – 5884.
[47] G. Oriji, Y. Katayama, T. Miura, *Electrochim. Acta* **2004**, *49*, 3091 – 3095.
[48] H. Wang, B. Qi, B. Lu, X. Bo, L. Guo, *Electrochim. Acta* **2011**, *56*, 3042 – 3048.
[49] M. J. Watt-Smith, S. P. Rigby, T. R. Ralph, F. C. Walsh, *J. Power Sources* **2008**, *184*, 29 – 37.

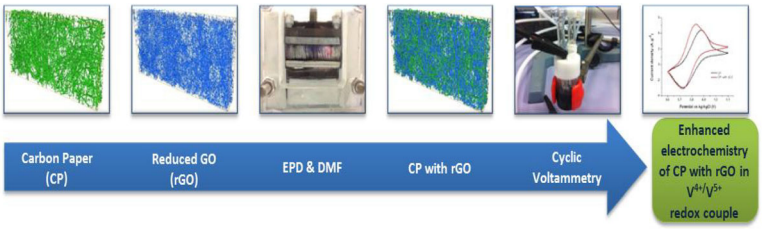
Manuscript received: July 8, 2016
Accepted Article published: September 29, 2016
Final Article published: ■■ ▮▮, 2016

 © 2016 The Authors. Published by Wiley-VCH Verlag GmbH & Co. KGaA, Weinheim

B. Chakrabarti,* D. Nir, V. Yufit, F. Tariq, J. Rubio-Garcia, R. Maher, A. Kucernak, P. Aravind, N. Brandon

■■ – ■■

Performance Enhancement of Reduced Graphene Oxide-Modified Carbon Electrodes for Vanadium Redox-Flow Systems



X-ray vision: Carbon paper (CP) electrodes are modified with reduced graphene oxide (rGO) by using electrophoretic deposition. X-ray tomography is used for the first time to characterize the deposits that result in enhanced charge-transfer performance for the VO^{2+}/VO_2^{+} redox couple.

© 2016 The Authors. Published by Wiley-VCH Verlag GmbH & Co. KGaA, Weinheim